Published in final edited form as:
J Phys Chem A. 2006 December 7; 110(48): 13089–13098. doi:10.1021/jp0632236.

A DFT/TDDFT Study of Lanthanide^{III} Mono- and Bis-Porphyrin Complexes

Meng-Sheng Liao, **John D. Watts**, and **Ming-Ju Huang***
Department of Chemistry, P.O. Box 17910, Jackson State University, Jackson, MS 39217

Abstract

Electronic structure, molecular structure, and electronic spectra of lanthanide^{III} mono- and bis-porphyrin complexes are investigated using a DFT/TDDFT method. These complexes include YbP(acac), YbP_2, $[YbP_2]^+$, $YbHP_2$, and $[YbP_2]^-$ (where P = porphine and acac = acetylacetonate). To shed some light on the origin of the out-of-plane displacement of Yb in YbP(acac), unligated model systems, namely planar D_{4h} and distorted C_{4v} YbP, were calculated. For comparison, the calculations were also extended to include the $Ce^{IV}P_2$ and $[Ce^{IV}P_2]^+$ systems. Even without an axial ligand, the lanthanide atom lies considerably above the porphyrin plane; the distortion of the YbP molecular structure from a planar D_{4h} to the non-planar C_{4v} symmetry leads to a considerable energy lowering. The axial ligand makes the metal out-of-plane displacement even larger, and it also changes the redox properties of the lanthanide mono-porphyrin. The ground state configurations of YbP_2 and $YbHP_2$ were determined by considering several possible low-lying states. YbP_2 is confirmed to be a single-hole radical. The special redox properties of the bis-porphyrin complexes can well be accounted for by the calculated ionization potentials and electron affinities. The TDDFT results provide a clear description of the UV-visible and near-IR absorption spectra of the various lanthanide porphyrins.

1. Introduction

Metal porphyrins (MPors) have been the subject of intense research because of their great biological importance and the unique nature of their coordination chemistry. (Here, we use Por to refer to any porphyrin.) While experimental studies of MPors have been expanded by the synthesis and characterization of species containing heavy metals, lanthanides, and actinides, theoretical studies have mainly been devoted to the first-row transition metal porphyrins. The combination of lanthanides (Ln) with porphyrins results in two different classes of interesting complexes: the lanthanide mono-porphyrinates[1a] and the lanthanide "sandwich" bis-porphyrinates. [1b] Since the lanthanides are too large to fit into the constrained porphyrin core, a large out-of-plane displacement of the metal in lanthanide porphyrins has been observed. Lanthanide mono-porphyrins exist always in the form of $LnPor(L)_n$, where L is an axial ligand; they have been studied as luminescent centers in near infrared (IR) polymer electroluminescent devices,[2–5] photochemical probes,[6,7] NMR dipolar probe and shift reagents,[8–10] contrast agents,[11] as well as electroactive materials for ion-sensitive electrodes.[12] Iwase and Igarashi reported electrochemical behaviors of a series of LnTPP(acac) complexes.[13]

In lanthanide bis-porphyrins $Ln(Por)_2$, the Ln atom holds two macrocycles close together. Strong electronic interactions between the porphyrins in the stacked porphyrins impart unique properties to these systems. Complexes of this type are proving useful as structural models of the photosynthetic reaction center in bacteria, and they possess spectroscopic and electrochemical properties similar to those of the special pair of *Rhodopseudomonas Viridis*.

*Corresponding author (email: mhuang@chem.jsums.edu).

[14,15] As a result, there have been many experimental studies of the $M(Por)_2$ compounds in recent years.[16–25] They are also of interest because of their electrochromic, semiconducting, and non-linear optical properties.[26] Compared to analogous monoporphyrins, there are two notable features of $M(Por)_2$: a blue shift of the B (or Soret) bands and a decrease in the oxidation potential.[16,17] In addition, the porphyrin sandwich compounds have a number of characteristic optical properties that are not exhibited by mono-porphyrins or dimers having larger spacing between the rings. For example, $Ln^{III}(Por)_2$ or the π-radical cations, $[M^{IV}(Por)_2]^+$ (formed by oxidation), exhibit an intense broad band in the near-IR region (1000 – 1400 nm)[20,22] not found in simple MPor or $[MPor]^+$. This near-IR absorption was proposed to arise from an electronic transition between the porphyrin-porphyrin bonding and antibonding orbitals.[20] Bucher and Scharbert measured optical spectra of the whole series of compounds $Ln(OEP)_2$ (Ln = La – Lu).[22]

Theoretical investigations on lanthanide porphyrins are very rare. A recent calculation on the cerium bis-porphine, CeP_2, was reported by Ricciardi et al.[27] The electronic structure of CeP_2 is relatively simple with a closed-shell ground state, where the oxidation state of Ce is +4. For other lanthanide bis-porphyrins, however, the oxidation state of Ln is +3. In this case, the ground state is, in essence, a ring → metal charge transfer (CT) state; one electron has been transferred from the porphyrin ring(s) to the metal to form a neutral complex. Different from the closed-shell $Ce^{IV}(Por)_2$ species, $Ln^{III}(Por)_2$ contains a single hole in the porphyrin π system. A notable characteristic of the single-hole species is a near-IR absorption band.[20, 22] The electronic structures of the $Ln^{III}(Por)_2$ complexes have not been explored in detail. To our knowledge, no theoretical studies of $LnPor(L)_n$ have been performed so far.

This paper comprises a density functional theory/time-dependent density functional theory (DFT/TDDFT) study of the YbP(acac), YbP_2, $YbHP_2$, and $[YbP_2]^-$ complexes, where P stands for the simple porphine and *acac* designates the bi-dentate ligand, acetylacetonate. The molecular structures of the complexes are illustrated in Figure 1. They share the common feature that the lanthanide atom sits above the porphyrin plane. Normal, transition metal porphines are planar (Figure 1a). The Pors used in experiments were tetraphenylporphine (TPP) and octaethylporphine (OEP). Previous calculations[28] have shown that the smaller P is able to mimic the essential properties of the more complicated species.

Spyroulias et al.[29–32] also reported synthesis and (optical and electrochemical) characterization of protonated forms of double-deckers, namely $LnH(Por)_2$ for Ln = Nd – Lu, where the H atom was suggested to reside atop one of the porphyrin rings.[31] For the asymmetrical complexes, one group of the four pyrrole nitrogens is not equal to another. In a basic solvent such as DMF or pyridine, the proton is abstracted, leading to a deprotonated form $[Ln(Por)]^-$.[29] To examine the influence of the axial hydrogen on the properties of the double-deckers, our calculations were extended to include the $YbHP_2$ and $[YbP_2]^-$ systems. In addition, to see the difference between $Ln^{III}(Por)_2$ and $Ce^{IV}(Por)_2$, results for CeP_2 and $[CeP]^+$ were also presented.

The main aim of this work is twofold:

- **i.** To provide a detailed description of the ground-state electronic structures of the mentioned ytterbium porphyrin complexes and their precise structural information. Accurate structural parameters for LnPor(acac) are unknown although the NMR spectra confirm the formation of paramagnetic metal porphyrins with the metal considerably displaced from the porphyrin plane.
- **ii.** To provide a quantitative interpretation for the spectral properties of the systems.

2. Computational Details

All calculations were carried out using the Amsterdam Density Functional (ADF) program package – ADF2005.01.[33–36] The STO basis set employed is the standard ADF-TZP, which is triple-zeta for valence orbitals plus one polarization function. To obtain accurate results, the valence set on the lanthanides included sub-valence 5s and 5p shells. For N, C, and O, 2s and 2p were considered as valence shells. The other shells of lower energy, i.e. [Kr]4d^{10} for Yb/Ce and [He] for N/C/O, were described as core and kept frozen according to the frozen-core approximation.[33] Among the various exchange-correlation potentials available, the density-parameterization form of Vosko, Wilk, and Nusair (VWN)[37] plus Becke's gradient correction for exchange (B)[38] and Perdew's gradient correction for correlation (P)[39] were employed. It has been shown that the combined VWN-B-P functional can give accurate bonding energies for both main-group[40] and transition metal[41] systems. Relativistic corrections of the valence electrons were calculated by the quasi-relativistic (QR) method.[42] (The relativistic corrections of atomic cores are taken into account at the Dirac-Fock level.) In this scalar (one-component) approach, spin-orbit (SO) coupling is not taken into account. Because SO effects are mainly atomic in nature, they are not expected to have significant influence on molecular properties[43] except metal-ligand binding energies.[44] Calculations on open-shell systems were performed using the spin-unrestricted method.

Electron excitation energies related to the electronic absorption spectra were calculated using the time-dependent density functional response theory (TDDFT)[45] as implemented in the ADF program. TDDFT provides a first-principles method for the calculation of excitation energies and presents an excellent alternative to the conventional highly correlated configuration interaction (CI) method. The recent implementation of TDDFT in the updated ADF program allows calculations of excitation energies for open-shell systems.

The ionization potentials (IPs) and electron affinities (EAs) were calculated by the so-called ΔSCF method in which separate SCF calculations for the neutral molecule and its ion are carried out and IP = $E(X^+) - E(X)$ and EA = $E(X^-) - E(X)$. The ionized and reduced species were re-optimized, but they are shown to undergo little geometry change as compared to the neutral species (see Table 3).

As mentioned in the Introduction, one aim of the present work is to provide precise structural information on ytterbium porphyrin complexes. Actually, the molecular structure of each system studied here has been optimized in order to obtain the "correct" electronic structure and energetic properties. The geometry optimization was done within certain symmetry specified for the system, and the choice of the symmetry is based on the most probable geometries of the molecule and the available X-ray crystal structures of comparable compounds. As the present model porphyrins are highly symmetric and rigid, the geometry optimization can be expected to converge to a minimum. The good agreement between the calculated and available experimental bond lengths and angles supports this point of view.

3. Results and Discussion

3.1. Electronic structure, structural, and energetic properties

3.1.1. YbP(acac)—For comparison, we also calculated two model systems of unligated YbP, which are in square planar D_{4h} and distorted C_{4v} symmetries, respectively. Figure 2 illustrates the changes of electronic structure from YbP (D_{4h}) to YbP (C_{4v}) to YbP(acac) (C_{2v}). With a $4f^{10}6s^2$ configuration for Yb, the ground state of YbP is a closed-shell state. The highest occupied molecular orbitals (HOMOs) are a set of 4f-orbitals. As pointed out in the Introduction, lanthanides do not form in-plane complexes with (normal) porphyrins, which may be attributed to a poor match between the atomic size and the macrocycle cavity diameter.

In planar YbP (YbP-D_{4h}), the relatively small core size of P results in a large σ-donor interaction that elevates the lanthanide 4f-orbitals greatly so that they lie considerably above the porphyrin a_{2u} orbital. When the central metal moves out of the plane, the σ-donor interaction is reduced and the 4f-orbitals are shifted down. When YbP is ligated by *acac*, the axial ligand abstracts an electron from the 4f-orbitals and so the 4f-orbitals are further lowered and now located around the porphyrin a_{2u} and a_{1u} orbitals in YbP(acac). The degeneracy of the f-orbitals is split with a band width of ~0.2 eV. Although the axial ligand *acac* lowers the symmetry of YbP from C_{4v} to C_{2v}, no split is found between the 2e-derived orbitals, $25b_1$ and $21b_2$.

Table 1 presents the calculated properties for YbP-D_{4h}, YbP-C_{4v}, Yb(acac), and YbP(acac); they include various structural parameters (R,∠), Mulliken orbital populations (Yb-5d, Yb-4f), Mulliken atomic charge (Q), Yb-P binding energies (E_{bind}), ionization potentials (IP), and electron affinities (EA). E_{bind} is defined as

$$-E_{bind}=E(YbP)-\{E(Yb)+E(P)\},$$

where E(YbP), E(Yb), and E(P) are the total energies of the indicated species. (The E_{bind} is not corrected with the zero point energy, which is expected to be small for the relatively large systems. That is, the vibration frequency of the Yb-P bond is expected to be low as both Yb and P are relatively large moieties.) $R_{Ct(N4)\ldots N}$ is a measure of the porphyrin core size and $R_{Ct(N4)\ldots Yb}$ represents the displacement of the metal out of the porphyrin plane.

The E_{bind} values indicate that distorted YbP-C_{4v} is ~ 1.6 eV more stable than planar YbP-D_{4h}, owing primarily to the energy lowering of the HOMOs. The displacement of Yb above the plane defined by the four pyrrole N-atoms is as large as 0.87 Å. Figure 3 illustrates the change of the relative energy of YbP with the motion of the metal out of the plane. (At each fixed R, the structure of YbP was re-optimized under C_{4v} symmetry.) The potential curve shows the Yb atom has a strong tendency to move out of the porphyrin plane. $R_{Ct(N4)\ldots Yb}$ increases by ~0.16 Å when YbP is attached by *acac*. There are X-ray crystal structure data available for YbTPP(H_2O)(THF)(Cl), wherein Yb is displaced by 1.090 Å,[46] in good agreement with the calculation (1.04 Å). On the other hand, the calculated Yb-O distance (2.25 Å) and OYbO angle (75.4°) in YbP(acac) agree well with those (2.22 Å, 73.4°) estimated from crystallographic results on lanthanide β-diketonate complexes.[9] We also calculated the fragment system Yb(acac); it is shown that both the distance and angle change significantly on going from Yb(acac) to YbP(acac).

The gross Yb-5d population in YbP-C_{4v} is ~0.8 e, showing a large electron donation from the ring ligand lone pair to the metal ion; on the other hand, there is about 0.4-e back-donation from the metal 4f-orbitals to the ring, with the result that the positive charge on Yb in YbP-C_{4v} is ~1.7 e. Q_{Yb} is increased by only ~0.3 e from $Yb^{II}P$ to $Yb^{III}P$(acac).

The Yb–P binding energy in YbP-C_{4v} is estimated to be 9.7 eV. With the presence of *acac*, the Yb–P bond is destabilized by about 1 eV, owing to the strong binding between Yb and *acac*.

The first ionization of YbP-C_{4v} occurs from a high-lying f-orbital. In the case of YbP(acac), the energies of the f-orbitals are lowered greatly and so the first ionization now takes place from the porphyrin a_{2u} ($28a_1$), in agreement with electrochemical results that the center of oxidation of LnPor(acac) is on the porphyrin base.[13] The calculated first IP of YbP(acac) is ~0.4 eV larger than that of YbP, suggesting that the axial ligation makes the oxidation of the system more difficult. This ligation also changes the electron affinity and the character of the LUMO (lowest unoccupied MO). For YbP, the added electron goes into the high-lying, anti-bonding porphyrin 2e orbitals. In contrast, the added electron in YbP(acac) now occupies a low-lying f-orbital. Therefore, the EA of YbP(acac) is more than 1 eV higher than that of YbP.

3.1.2. YbP_2—$Ln(Por)_2$ is a sandwich-like complex in which the macrocycle rings are staggered by about 45° (Figure 1c). This symmetry has been well established by experiment, and our calculations show that the square antiprismatic D_{4d} conformation is indeed preferred over a face-to-face conformation which maintains D_{4h} symmetry (see Table 3). Another structural feature of $Ln(Por)_2$ is that both porphyrins are domed and severely distorted from planarity. This is also confirmed by the calculations. The saucer-like deformation of the macrocycle is necessary to improve the overlap of the porphyrin pair and to maximize the Ln-N interaction.

To determine the ground state for YbP_2, the energetics of several possible low-lying states were computed, whose relative energies are presented in Table 2. (Geometry optimization was performed for all states. The same is true for other molecules listed in Table 2.) According to the results, the lowest energy electronic configuration for YbP_2 is clearly $(12b_2/f)^1(5a_2)^1$, where one electron is located in a Yb-4f orbital and the other resides in a P_2 orbital. There seem to be no other competing low-lying states. Figure 4 illustrates the P, P_2, and YbP_2 orbital energy levels and their correlations. The P_2 MOs are formed from linear combination of the P MOs of appropriate symmetry; they are split into bonding and anti-bonding pairs. Interaction of the P-HOMOs (a_{1u}) leads to a large splitting and the bonding and anti-bonding MOs are b_1 and a_2, respectively. The two lowest unoccupied MOs (LUMOs) (a_{2u}) of P overlap to form the b_2 and a_1 orbitals, which split relatively weakly. In P_2, b_2 and a_2 become the HOMO and LUMO, respectively. For the higher-lying virtual orbitals of P_2, $2e_3$ and $2e_1$ are the bonding and anti-bonding MOs of the e_g* orbitals of mono-porphyrins.

Since in YbP_2 the $5a_2$ orbital is occupied by only one electron, the trivalent lanthanide sandwich complex contains a single hole in the P_2 π system and this hole is apparently delocalized through the P-P interaction. Therefore, there is net bonding interaction in the ground state of YbP_2. Under D_{4d} symmetry, the metal 4f-orbitals transform as b_2, e_1, e_2, and e_3 and they are split widely. There are no metal f-orbitals of appropriate symmetry to mix with the HOMO $5a_2$.

The orbital energy level diagram of CeP_2 is presented on the right-hand side in Figure 4. In this bis-porphyrin, seven unoccupied 4f-like orbitals ($15e_3$, $15e_2$, $16e_1$, $12b_2$) all lie well above the $5a_2$ orbital and they constitute the LUMOs. The ground state of CeP_2 is clearly $(5a_2)^2$, a closed-shell $^1A_1$ state. There is no single electron that occupies a 4f-orbital and so Ce in CeP_2 has the oxidation state of +4.

The calculated properties of ground state YbP_2 are presented in Table 3, together with the results of CeP_2 for comparison. Here E_{bind} is defined as

$$-E_{bind}=E(LnP_2)-\{E(Ln)+2E(P)\},$$

which provides one measure of the extent of π-π overlap interaction in LnP_2. As mentioned above, the porphyrin in LnP_2 adopts a domed conformation. $R_{Ct(N4)\ldots Ct(H8)}$ is a direct measure of the doming in such complexes. We also presented in the table the distance between the N4 and C8 planes, $R_{Ct(N4)\ldots Ct(C8)}$.

The Yb-atom in YbP_2 sits 1.37 Å above the centroid of the plane defined by the four pyrrole N-atoms. This is larger than the displacement of the metal in YbP(acac) (1.04 Å). The doming defined by $R_{Ct(N4)\ldots Ct(H8)}$ is as large as 0.73 Å. In Table 3, $R_{P\text{-}P}$ represents the P–P distance, which is taken as the distance between the planes defined by the four N-atoms of each ring. According to this definition, the two macrocycles in YbP_2 are separated by 2.75 Å. The total height of the molecule as measured from one H8 plane to another H8 plane is 4.2 Å. As Ce^{IV} is bigger than Yb^{III} (1.01 Å vs. 0.94 Å), the calculated structural parameters for CeP_2 are all slightly larger than those for YbP_2; even the doming is larger in CeP_2 than in YbP_2. There

are X-ray crystal structure data available for the OEP substituted sandwich $Ce(OEP)_2$,[25] which are in good agreement with the calculation.

The Ln-P_2 binding energy is large, 14.1 eV for YbP_2 and 19.3 eV for CeP_2. This accounts for the high stability of the $Ln(Por)_2$ complexes.

According to the calculation, the first ionization occurs from the $5a_2$ orbital. Thus, one-electron oxidation of $Yb(Por)_2$ will produce a double-hole $[Yb(Por)_2]^+$ species. The second hole resides in the same MO as the first hole, consistent with a resonance Raman (RR) spectroscopy study:[19] Electron spin resonance (ESR) spectra recorded for the two-hole complexes also suggested no unpaired electrons reside in the porphyrin π-π system at room or low temperature.[19] As sandwich porphyrin cations have been the subject of experimental studies,[18,19,22] Table 3 also reports the optimized structural parameters for $[YbP_2]^+$, which indicate that the positive ion is slightly 'tighter' than the neutral species because removal of an electron from the anti-bonding dimer MO would increase the net π-π bond order in the ground state. Owing to the anti-bonding character of the $5a_2$ orbital, the calculated first IP of the dimer (6.02 eV) is significantly smaller than that of the monomer (6.62 eV), in agreement with the experimental result that oxidation of $Ln(Por)_2$ is remarkably easy compared to that of MPor.

Concerning the reduction, the added electron in YbP_2 occupies the P_2-$5a_2$ orbital and the calculated EA is very negative (−2.98 eV). This is in contrast to YbP(acac). Addition of an electron to the 4f-like orbital $12b_2$ yields a significantly smaller EA. This is again in accord with the experimental fact that $Ln^{III}(Por)_2$ is much easier to reduce than the corresponding monoporphyrin.[16] In the case of $Ce^{IV}P_2$, the reduction involves addition of an electron to the LUMO ($15e_3$/f), giving the anion with Ce^{III}.

$[CeP_2]^+$ has a ground state configuration of $(5a_2)^1$. Therefore, neutral YbP_2 is electronically similar to the Ce^{IV} sandwich porphyrin cation radical. The structural change from CeP_2 to $[CeP_2]^+$ is smaller than that from YbP_2 to $[YbP_2]^+$.

3.1.3. $YbHP_2$—The ground state of $YbHP_2$, $(15b_2/f)^1(10a_2)^2$, actually corresponds to that of YbP_2 by addition of one electron to $5a_2$. Thus, the oxidation state of Yb in $YbHP_2$ is still +3. Magnetic susceptibility measurements of $YbH(Por)_2$ yield values of magnetic moments typical for the trivalent oxidation state.[29] The experimental result is supported by the calculation. A $(15b_2/f)^2(10a_2)^1$ state is 0.43 eV higher in energy (see Table 2). With the $10a_2$ orbital doubly occupied, $YbH(Por)_2$ is no longer a π-radical. This was verified through ESR spectroscopy in solution and pure solid.[29] The orbital energy level diagram of $YbHP_2$ is illustrated in Figure 4. There is a large downshift of the 4f-like orbitals on going from YbP_2 to $YbHP_2$ so that these orbitals now fall well below the porphyrin $10a_2$ and $23a_1$ orbitals.

As illustrated in Figure 1d, the molecular structure of $YbHP_2$ is asymmetric, where one porphyrin is bonded with an axial H-atom and other one is not. The complex may be expressed as Yb(HP)(P), where the porphyrin (P) and the protonated porphyrin (HP) represent different subunits. Table 3 shows that the distances from Yb to the N4 planes of HP and P are rather different, with $R_{Ct(N4)\ldots Yb}$ in HP being larger than that in P. Correspondingly, the core size ($R_{Ct(N4)\ldots N}$) of HP is somewhat smaller than that of P. But the doming of the ring is more significant in HP than in P.

Owing to a small downshift of the valence P_2-a_2 orbital, the calculated first IP of $YbHP_2$ is also slightly larger than that of YbP_2. The reduction of $YbHP_2$ now involves addition of an electron to the 4f-like orbital $15b_2$, and the calculated EA for this complex is smaller than that for YbP_2. The negative ion $[YbP_2]^-$ has the same ground state as $YbHP_2$ does, and so it is also

not a π-radical. The non-radical character of $[Yb(Por)_2]^-$ is supported by the optical properties since no near-IR band was detected (see section B.3).

3.2. Electron excitation energies

Table 4 – Table 9 report the TDDFT calculated excitation energies (E^{exc}) and oscillator strengths (*f*) for the allowed transitions from the ground state to excited states in YbP(acac), YbP_2, CeP_2, $[CeP_2]^+$, $YbHP_2$, and $[YbP_2]^-$, respectively. Experimental data[13,21,22,29] for each system are provided for comparison.

3.2.1. YbP(acac)—For a "normal" planar metal porphyrin (e.g. MgPor, NiPor, or ZnPor), the HOMO and HOMO-1 are the porphyrin a_{2u} and a_{1u}, respectively, which are nearly degenerate and well separated from lower-lying levels. The excitations from the (a_{2u}, a_{1u}) to the LUMO (e_g), which lead to the two lowest excited states 1^1E_u and 2^1E_u, give rise to a weak absorption band Q in the visible and a very strong B (or Soret) band in the near ultraviolet (UV).[47] (For the a_{1u}, a_{2u}, and e_g orbitals mentioned here, refer to the orbital energy level diagram of YbP-D_{4h} in Figure 2).

Experimental spectral data are available for YbTPP(acac)[13] and are shown to be different from those of a normal MPor. They exhibit two weak absorption bands (assigned as Q′ and Q) and two strong absorption bands (assigned as B and B′). The multiple bands in the Q and B regions are supported by the calculations on YbP(acac). Because there is no split between the $25b_1$ and $21b_2$ orbitals, the excitation energies for the transitions from an orbital to $25b_1$ and $21b_2$ are the same or nearly the same. The Q′ and Q bands are assigned to the $9^2B_1/4^2B_2$ and $8^2B_2/13^2B_1$ states, respectively, which are nearly pure $14a_2 \rightarrow 21b_2/25b_1$ and $28a_1 \rightarrow 21b_2/25b_1$ transitions. Here, $14a_2$ and $28a_1$ are the porphyrin a_{1u} and a_{2u} orbitals, respectively. For a normal MPor, a_{1u} and a_{2u} are nearly degenerate and the Q and B bands just arise from a mixture of the $a_{1u} \rightarrow e_g$ and $a_{2u} \rightarrow e_g$ transitions; that is, Q is described by a plus combination of the $a_{1u} \rightarrow e_g$ and $a_{2u} \rightarrow e_g$ transitions while B is described by a minus combination of the $a_{1u} \rightarrow e_g$ and $a_{2u} \rightarrow e_g$ transitions. In the case of YbP(acac), the $14a_2$ and $28a_1$ orbitals are separated relatively widely and the $14a_2 \rightarrow 21b_2/25b_1$ and $28a_1 \rightarrow 21b_2/25b_1$ transitions do not mix, which give rise to just two weak Q bands. Our calculated oscillator strength (*f*) for the Q′ band is nearly zero and it may be underestimated by the TDDFT method. We find that there is a ring to metal (R → M) transition, i.e. $19b_1 \rightarrow 24b_1$, occurring at 2.08 eV with *f* = 0.005. It is possible that the Q′ band results from this transition. Since the 4f-shell is open, there exist several R → M transitions with non-negligible *f* to the red of the Q bands. They occur at 0.75, 1.71, and 1.86 eV respectively and should contribute to the near-IR region of YbPor (acac). There are also 4f → 4f transitions, which have low excitation energies and very small oscillator strengths.

Based on the calculated E_{exc} and *f*, the two strong B and B′ bands are assigned to the $13^2B_2/19^2B_1$ and $21^2B_1/14^2B_2$ states, respectively; the former arises from a mixture of the $28a_1 \rightarrow 21b_2/25b_1$ and $27a_1 \rightarrow 21b_2/25b_1$ transitions while the latter is mainly from the $27a_1 \rightarrow 21b_2/25b_1$ transition. According to the calculations, several transitions with large *f* are present to the blue of the B bands. But there has been no experimental elucidation of any details about this energy region. Between the Q and B bands, there are some M → R and R → M transitions, which may only contribute to the broadening of the Q or B band. The calculated excitation energies for YbP(acac) are generally 0.2 – 0.3 eV larger than the spectral data for YbTPP(acac). (For the Q′ band, the calculated and experimental results are almost equal.)

3.2.2. YbP_2—Experimental spectral data are available for $Yb(OEP)_2$ and show three weak bands, assigned as Q_1, Q_2, and Q_3, and one strong band, assigned as B.[22] In addition, there is an intermediately strong band at a low energy of 1.08 eV. The presence of an intense near-IR

absorption is a remarkable feature of the single-hole $Ln^{III}(Por)_2$ and $[Ce^{IV}(Por)_2]^+$ species, and is attributed to a transition between the two delocalized MOs, namely $5b_1 \rightarrow 5a_2$. This is a consequence of the orbital splitting due to ring-ring interaction. Our calculated E^{exc} (1.15 eV) and *f* (0.0713) for the $5b_1 \rightarrow 5a_2$ transition nicely account for this near-IR absorption.

The Q_1 band is assigned to the 11^3E_1 state, which is dominated by the $5a_2 \rightarrow 17e_1$ transition (~60%) and includes some participation of the $14e_1 \rightarrow 5a_2$ transition (~30%). Since $5a_2$ is an anti-bonding orbital and lies relatively high, the Q_1 band here is red-shifted with respect to the Q′ band of YbP(acac). The Q_2 and Q_3 bands are accounted for by the $5b_1 \rightarrow 16e_3$ and $11b_2 \rightarrow 16e_3$ transitions, respectively. The 30^3E_1 state (E^{exc} = 3.65 eV, *f* = 0.3866) is then responsible for the B band, which shows a large mixture of the $13e_2 \rightarrow 16e_3$ and $16e_1 \rightarrow 16e_2$ transitions. There are several R → M and M → R transitions occurring to the red of the Q bands.

The general appearance of the spectrum of $Ce(OEP)_2$ is similar to that of $Yb(OEP)_2$ (three weak Q bands and one strong B band), including the absorption maximum positions.[21] This is consistent with the calculations on YbP_2 and CeP_2. With a doubly occupied $5a_2$ orbital, the CeP_2 species does on longer have a characteristic near-IR absorption, different from YbP_2.

In contrast to neutral $Ce(OEP)_2$, the absorption spectrum of $[Ce(OEP)_2]^+$ is relatively simple; it exhibits one Q band and one B band.[21] In the cation π-radical, the $5b_1 \rightarrow 5a_2$ transition results in a strong near-IR absorption feature, similar to the situation for $Yb(Por)_2$. The calculated E^{exc} for this transition (1.02 eV) is close to that observed for $[Ce(OEP)_2]^+$ (0.98 eV). There is a blue-shift of the B band from $Ce(OEP)_2$ to $[Ce(OEP)_2]^+$; the same trend is obtained from the calculation.

3.2.3. $YbHP_2$—The experimental spectral data given in Table 8 for comparison are those measured for $YbH(TPP)_2$.[29] They show three weak Q bands and a single strong B band. This is similar to $Yb(OEP)_2$. But the protonated complex no longer has the characteristic near-IR absorption according to the calculation, in agreement with the experimental non-observation.[29] The addition of a H-atom to $Yb(Por)_2$ also produces a significant red-shift in the B band, as indicated by both calculation and experiment.

$[Yb(TPP)_2]^-$ has a similar ground state to $YbH(TPP)_2$ but its spectral data display significant differences.[29] They consist of six Q bands in addition to a single B band. These bands are assigned to the 11^2E_1, 13^2E_1, 14^2E_1, 17^2E_1, 18^2E_1, 20^2E_1, 24^2E_1 states respectively according to our calculation. Also, $[Yb(Por)_2]^-$ does not exhibit a strong near-IR absorption band.

4. Conclusions

Even unligated YbP is non-planar with the lanthanide atom lying considerably above the porphyrin plane. The axial ligand *acac* in YbP(acac) makes the metal out-of-plane displacement even larger, and it also changes the redox properties of the lanthanide mono-porphyrin. The one-electron oxidation and reduction of YbP occur from the metal and porphyrin ring, respectively, but the opposite situations are found for YbP(acac). Both the first ionization potential (IP) and electron affinity (EA) are increased on going from YbP to YbP (acac).

The orbital energy level diagrams provide insight into the electronic structure of the lanthanide^{III} bis-porphyrin complexes. The ground state configurations of YbP_2 and $YbHP_2$ are determined to be $(b_2/f)^1(a_2)^1$ and $(b_2/f)^1(a_2)^2$, respectively, where b_2 is a metal 4f-like orbital and a_2 is derived from the overlapping of the porphyrin a_{1u} orbitals. Therefore, YbP_2 is a single-hole π-radical, similar to $[Ce^{IV}P_2]^+$. Both one-electron oxidation and reduction of YbP_2 all occur from the a_2 orbital. The first IP is relatively small while the EA is large, which

accounts for the ease of both oxidation and reduction for the porphyrin π-π system. The experimental predictions of the ground states of $Yb(Por)_2$, $[Yb(Por)_2]^+$, $YbH(Por)_2$, $[Yb(Por)_2]^-$ are supported by the calculations. The large interaction between Ln and P_2 accounts for the high stability of the $Ln(Por)_2$ complexes.

The calculated excitation energies and oscillator strengths are generally in good agreement with the experimental spectral data. In contrast to a normal, square planar metal porphyrin (MPor), the spectrum of a lanthanide porphyrin (whether it is a mono- or bis-porphyrin) is more complicated; it contains a number of weak, low-energy absorptions to the red of the Q band. In YbP(acac), the near-degeneracy of the porphyrin a_{1u} and a_{2u} orbitals is lifted; the $a_{1u} \rightarrow$ LUMO and $a_{2u} \rightarrow$ LUMO transitions become almost pure, which give rise to the Q′ and Q bands respectively. The spectrum of YbPor(acac) also exhibits two B bands, which are shown to result from a significant mixture of several transitions from lower-lying orbitals to the LUMOs. In the bis-porphyrins, the strong π-π interaction between the two macrocycles results in the appearance of new optical features including a number of Q bands for $[YbP_2]^-$ and the strong near-IR absorption for YbP_2 and $[CeP_2]^+$. The origin and nature of the B bands of the bis-porphyrins are also different from those of a normal MPor.

Finally, our optimized structures of the various ytterbium porphyrins in this work would aid in future X-ray crystallographic studies of corresponding compounds.

Supplementary Material

Refer to Web version on PubMed Central for supplementary material.

Acknowledgments

This work was supported by the National Institutes of Health (NIH) grant (S06 GM08047), the National Science Foundation (NSF) CREST grant (HRD0318519), and by the NSF-EPSCoR grant (NSF300423-190200-21000). The ADF calculations were run on a QuantumCube™ QS4-2800C computer from Parallel Quantum Solutions, LLC.

References and Notes

1. (a) Wong C-P, Horrocks DW Jr. Tetrahedron Lett 1975:2637. (b) Buchler JW, Elsässer K, Kihn-Botulinski M, Scharbert B. Angew. Chem. Int. Ed. Engl 1986;25:286.
2. Harrison BS, Foley TJ, Bouguettaya M, Boncella JM, Reynolds JR, Schanze KS, Shim J, Holloway PH, Padmanaban G, Ramakrishnan S. Appl. Phys. Lett 2001;79:3770.
3. Foley TJ, Harrison BS, Knefely AS, Abboud KA, Reynolds JR, Schanze KS, Boncella JM. Inorg. Chem 2000;42:5023. [PubMed: 12895128]
4. Foley TJ, Abboud KA, Boncella JM. Inorg. Chem 2002;41:1704. [PubMed: 11925160]
5. He HS, Wong W-K, Li K-F, Cheah K-W. Synthetic Metals 2004;143:81.
6. Martarano LA, Wong C-P, Horrocks WD, Goncalves AMP. J. Phys. Chem 1976;80:2389.
7. Gouterman M, Schumaker CD, Srivastava TS, Yotenani T. Chem. Phys. Lett 1976;40:456.
8. Horrocks WD, Hove EG. J. Am. Chem. Soc 1978;100:4386.
9. Horrocks WD, Wong C-P. J. Am. Chem. Soc 1976;98:7157. [PubMed: 977867]
10. Wong C-P, Venteicher RF, Horrocks WD. J. Am. Chem. Soc 1974;96:7149. [PubMed: 4373496]
11. Lauffer RB. Chem. Rev 1987;87:901.
12. Zhang X-B, Guo C-C, Xu J-B, Shen G-L, Yu R-Q. Analyst 2000;125:867. [PubMed: 10885056]
13. Iwase A, Igarashi A. Electrochim. Acta 1993;38:689.
14. Parson WW, Warshel A. J. Am. Chem. Soc 1987;109:6152.
15. Tran-Thai T-H, Mattioli TA, Chabach D, DeCian A, Weiss R. J. Phys. Chem 1994;98:8279.
16. Collman JP, Kendall JL, Chen JL, Collins KA, Marchon J-C. Inorg. Chem 2000;39:1661. [PubMed: 12526551]

17. Bilsel O, Rodrguez J, Milam SN, Gorlin PA, Girolami GS, Suslick KS, Holten D. J. Am. Chem. Soc 1992;114:6528.
18. Perng J-H, Duchowski JK, Bocian DF. J. Phys. Chem 1991;95:1319.
19. Perng J-H, Duchowski JK, Bocian DF. J. Phys. Chem 1990;94:6684.
20. Duchowski JK, Bocian DF. J. Am. Chem. Soc 1990;112:3312.
21. Donohoe RJ, Duchowski JK, Bocian DF. J. Am. Chem. Soc 1988;110:6119.
22. Buchler JW, Scharbert B. J. Am. Chem. Soc 1988;110:4272.
23. Buchler JW, deCian A, Fischer J, Kihn-Botulinski M, Weiss R. Inorg. Chem 1988;27:339.
24. Yan XW, Holten D. J. Phys. Chem 1988;92:409.
25. Buchler JW, deCian A, Fischer J, Kihn-Botulinski M, Paulus H, Weiss R. J. Am. Chem. Soc 1986;108:3652.
26. Dunford CL, Williamson BE, Krausz E. J. Phys. Chem. A 2000;104:3537.
27. Ricciardi G, Rosa A, Baerends EJ, van Gisbergen SAJ. J. Am. Chem. Soc 2002;124:12319. [PubMed: 12371876]
28. Liao M-S, Scheiner S. J. Chem. Phys 2002;116:3635.
29. Spyroulias GA, Raptopoulou CP, de Montauzon D, Mari A, Poilblanc R, Terzis A, Coutsolelos AG. Inorg. Chem 1999;38:1683. [PubMed: 11670935]
30. Bertini I, Coutsolelos A, Dikiy A, Luchinat C, Spyroulias GA, Troganis A. Inorg. Chem 1996;35:6308.
31. Spyroulias GA, Coutsolelos GA. Inorg. Chem 1996;35:1382. [PubMed: 11666337]
32. Spyroulias GA, Coutsolelos AG, Raptopoulou CP, Terzis A. Inorg. Chem 1995;34:2476.
33. Baerends EJ, Ellis DE, Roos P. Chem. Phys 1973;2:41.
34. te Velde G, Bickelhaupt FM, van Gisbergen SJA, Fonseca-Guerra C, Baerends EJ, Snijders JG, Ziegler T. J. Comput. Chem 2001;22:931.
35. Fonseca-Guerra C, Snijders JG, Baerends EJ, te Velde G. Theor. Chem. Acc 1998;99:391.
36. ADF2005.01; SCM: Theoretical Chemistry. Amsterdam, The Netherlands: Vrije Universiteit; http://www.scm.com
37. Vosko SH, Wilk L, Nusair M. Can. J. Phys 1980;58:1200.
38. Becke AD. Phys. Rev. A 1988;38:3098. [PubMed: 9900728]
39. Perdew JP. Phys. Rev. B 1986;33:8822.
40. Johnson BG, Gill PMW, Pople JA. J. Chem. Phys 1993;98:5612.
41. Li J, Schreckenbach G, Ziegler T. J. Am. Chem. Soc 1995;117:486.
42. Ziegler T, Tschinke V, Baerends EJ, Snijders JG, Ravenek W. J. Phys. Chem 1989;93:3050.
43. Zhou M-F, Andrews L, Ismail N, Marsden C. J. Phys. Chem. A 2000;104:5495.
44. Maron L, Leininger T, Schimmelpfennig B, Vallet V, Heully J-L, Teichteil C, Gropen O, Wahlgren U. Chem. Phys 1999;244:195.
45. van Gisbergen SJA, Snijders JG, Baerends EJ. Comput. Phys. Commun 1999;118:119.
46. Wong W-K, Zhang L-L, Wong W-T, Xue F, Mak TCW. J. Chem. Soc. – Dalton Trans 1999:615.
47. Rosa A, Ricciardi G, Baerends EJ, van Gisbergen SJA. J. Phys. Chem. A 2001;105:3311.

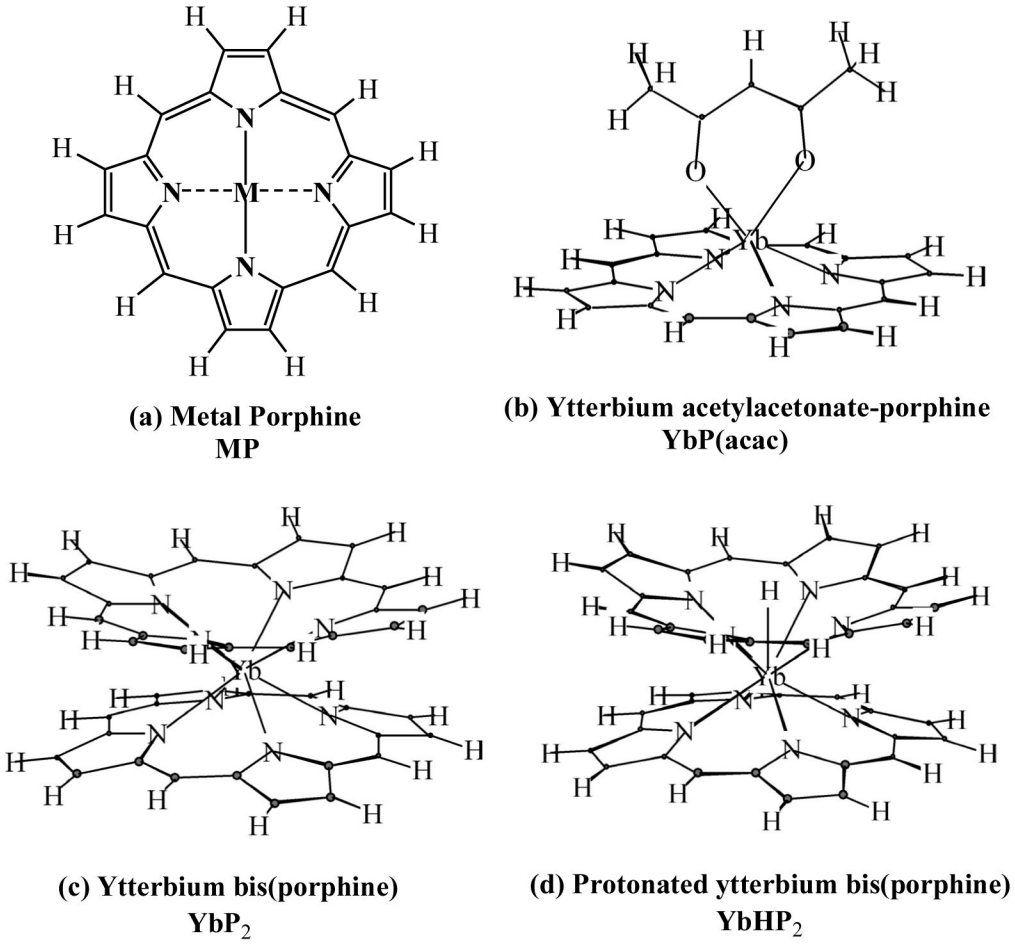

Figure 1.
Molecular structures of MP, YbP(acac), YbP_2, and $YbHP_2$.

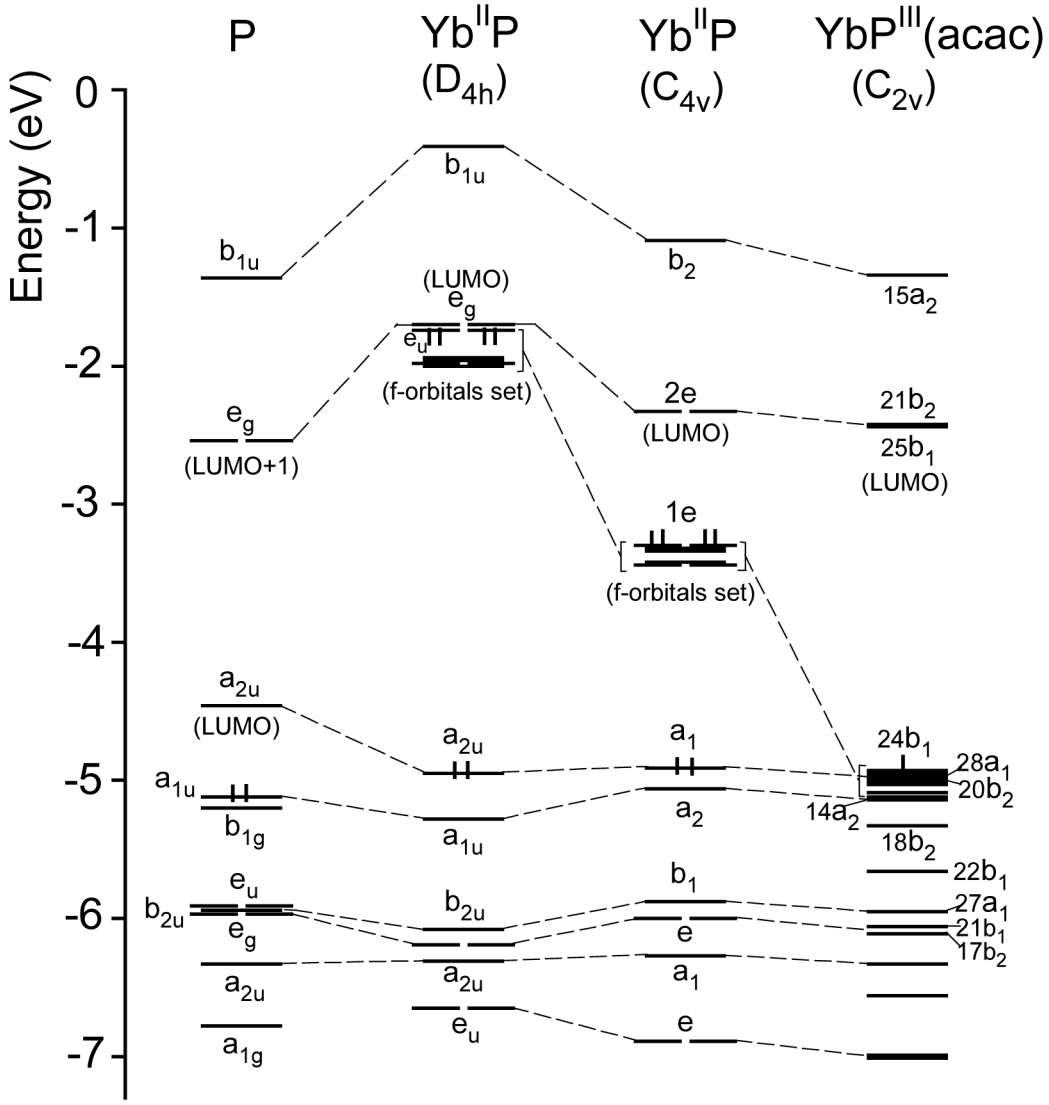

Figure 2.
Orbital energy levels for the valence orbitals of P, YbP-D_{4h}, YbP-C_{4v}, and YbP(acac).

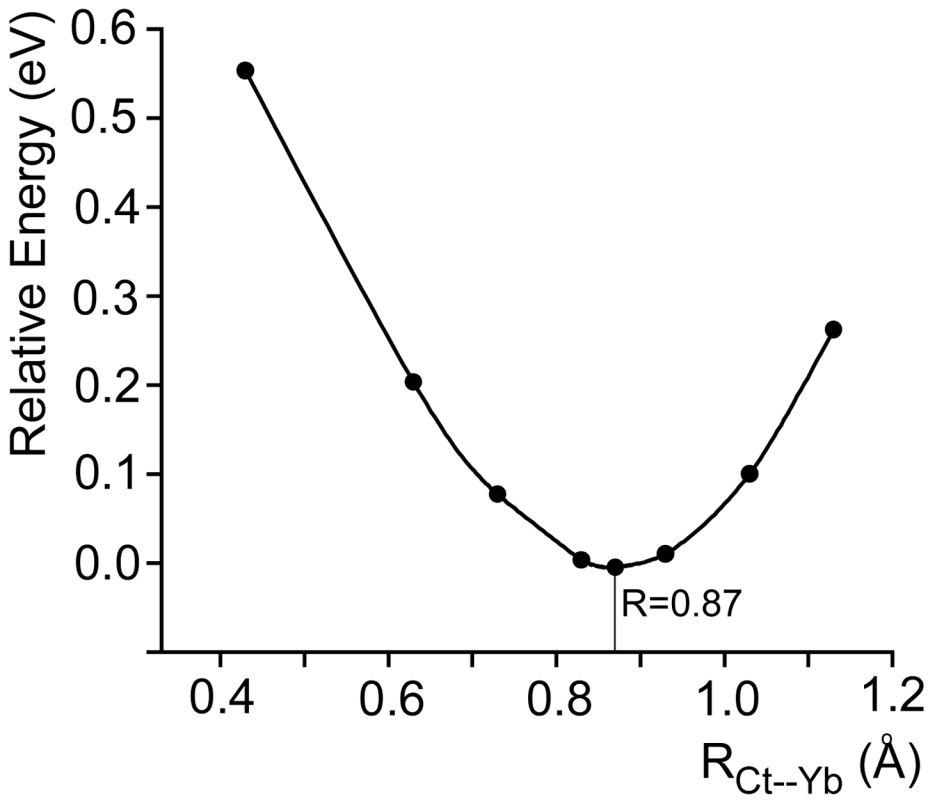

Figure 3.
Variation of the relative energy of YbP with the Yb out-of-plane displacement.

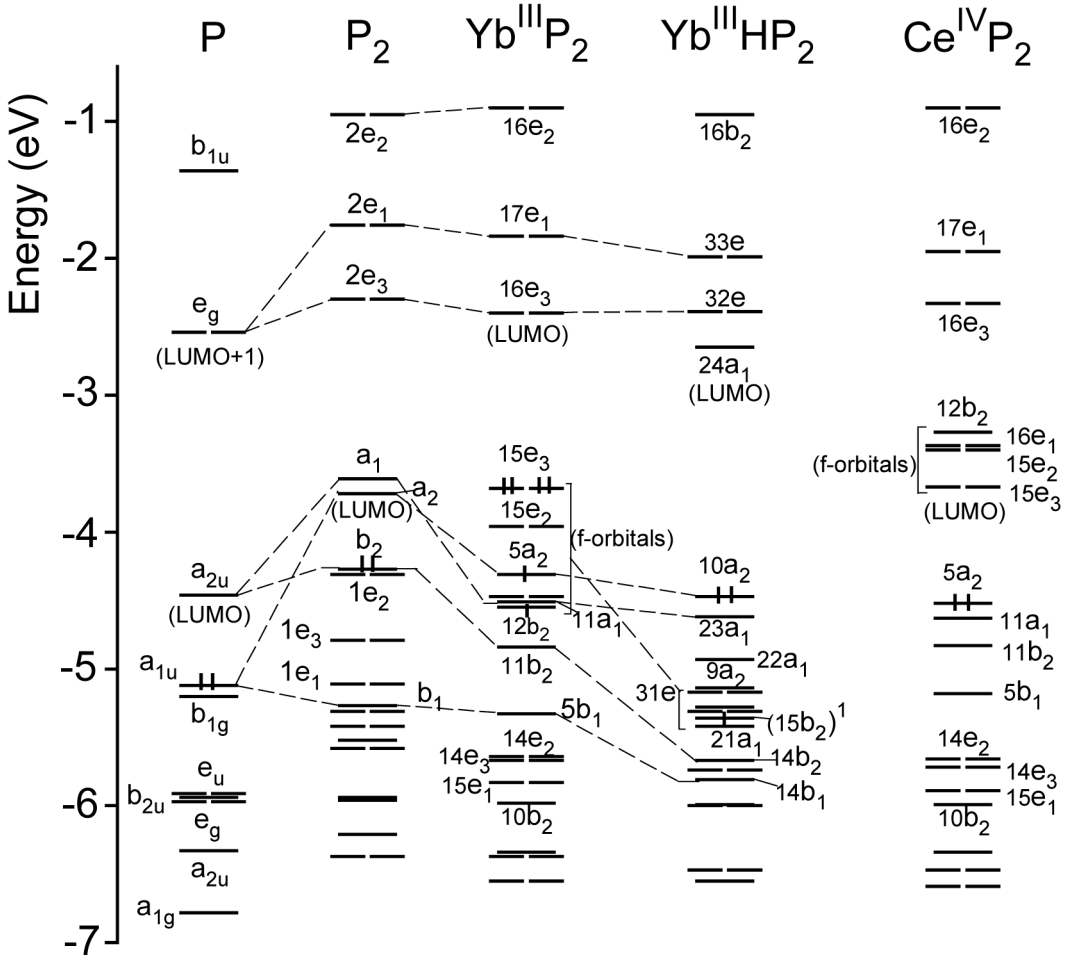

Figure 4.
Orbital energy levels for the valence orbitals of P, P_2, YbP_2, $YbHP_2$, and CeP_2.

Table 1

Calculated properties[a] of ytterbium mono-porphyrin complexes

	YbP (D_{4h})	YbP (C_{4v})	Yb(acac)	YbP(acac) (C_{2v})	
				Calc	Exptl
$R_{Yb\text{-}N}$, Å	2.204	2.264		2.321	2.326[c]
$R_{Ct(N4)\ldots N}$, Å[b]		2.089		2.076	2.055[c]
$R_{Ct(N4)\ldots Yb}$, Å		0.874		1.037	1.090[c]
$R_{Ct(N4)\ldots Ct(C8)}$, Å[b]		0.228		0.141	
$R_{Ct(N4)\ldots Ct(H8)}$, Å[b]		0.328		0.201	
$R_{Yb\text{-}O}$, Å			2.167	2.251	2.22[d]
∠OYbO, °			82.4	75.4	73.4[d]
Yb-5d, e	0.74	0.77	0.43	0.91	
Yb-4f, e	13.73	13.60	13.74	13.29	
Q_{Yb}	1.68	1.67	0.65	1.94	
E_{bind}(Yb-P), eV	8.08	9.65		8.70[e]	
IP, eV		6.27 (1e/f-like)		6.62 ($28a_1$)	
		6.74 (a_1)		7.35 ($20b_2$/f-like)	
EA, eV		−1.26 (2e)		−2.21 ($24b_1$/f-like)	
				−1.05 ($25b_1$)	

[a] R: distance, ∠: angle, Ln-5d/4f: Mulliken orbital population, Q: atomic charge, E_{bind} binding energy, IP: ionization potential, and EA: electron affinity.

[b] Ct(N4): centroid of the plane defined by the four pyrrole nitrogen atoms, Ct(C8): centroid of the plane defined by the eight peripheral carbon atoms, Ct(H8): centroid of the plane defined by the eight peripheral hydrogen atoms.

[c] X-ray crystal structure data on YbTPP(H_2O)(THF)(Cl) (ref. 46).

[d] Estimated from crystallographic results on lanthanide β-diketonate complexes (ref. 9).

[e] This binding energy is defined as $-E_{bind}$ = E[YbP(acac)] − E[Yb(acac)] − E(P).

Table 2

Calculated relative energies (E, eV) for selected configurations in YbP_2, CeP_2, and $YbHP_2$

System	Configuration[a]	Term	$E^{relative}$	Oxidation state on Ln
YbP_2	$(12b_2/f)^1(11a_1)^2(5a_2)^1(15e_3/f)^4$	$^3B_1$	0	Yb^{III}
	$(12b_2/f)^2(11a_1)^2(5a_2)^1(15e_3/f)^3$	$^3E_3$ (A)	0.57	Yb^{III}
	$(12b_2/f)^1(11a_1)^2(5a_2)^2(15e_3/f)^3$	$^3E_3$ (B)	0.77	Yb^{IV}
	$(12b_2/f)^2(11a_1)^2(5a_2)^0(15e_3/f)^4$	$^1A_1$	0.89	Yb^{II}
	$(12b_2/f)^2(11a_1)^1(5a_2)^1(15e_3/f)^4$	$^3A_2$	0.91	Yb^{II}
CeP_2	$(5a_2)^2$	$^1A_1$	0	Ce^{IV}
	$(5a_2)^1(15e_3)^1$	$^3E_3$	1.15	Ce^{III}
$YbHP_2$	$(15b_2)^1(15b_1)^2(31e)^4(23a_1)^2(10a_2)^2$	$^2B_2$	0	Yb^{III}
	$(15b_2)^2(15b_1)^1(31e)^4(23a_1)^2(10a_2)^2$	$^2B_1$	0.13	Yb^{III}
	$(15b_2)^2(15b_1)^2(31e)^3(23a_1)^2(10a_2)^2$	^2E	0.19	Yb^{III}
	$(15b_2)^2(15b_1)^2(31e)^4(23a_1)^2(10a_2)^1$	$^2A_2$	0.43	Yb^{II}
	$(15b_2)^2(15b_1)^2(31e)^4(23a_1)^1(10a_2)^2$	$^2A_1$	0.56	Yb^{II}

[a] See Figure 4 for the orbitals; here "f" means an f-like orbital.

Table 3

Calculated properties[a] of lanthanide bis-porphyrin complexes at the ground state

	$Yb^{III}P_2$	$Ce^{IV}P_2$		$[Yb^{III}P_2]^+$	$[Ce^{IV}P_2]^+$	$Yb^{III}HP_2$	$[Yb^{III}P_2]^-$
		Calc	Exptl[b]				
$\Delta E(D_{4d} - D_{4h})$, eV	−0.20	−0.38		−0.09	−0.28	−0.50	−0.44
$R_{Ln\text{-}N}$, Å	2.476	2.526	2.475	2.462	2.522	2.556, 2.409[c]	2.503
$R_{Ct(N4)\ldots N}$, Å[d]	2.060	2.077	2.057	2.055	2.079	2.029, 2.063	2.070
$R_{Ct(N4)\ldots Ln}$, Å	1.374	1.438	1.376	1.357	1.428	1.554, 1.244	1.407
$R_{Ct(N4)\ldots Ct(C8)}$, Å[d]	0.512	0.532		0.522	0.506	0.617, 0.526	0.540
$R_{Ct(N4)\ldots Ct(H8)}$, Å[d]	0.726	0.762		0.747	0.728	0.868, 0.728	0.763
$R_{P\text{-}P}$, Å[e]	2.748	2.876	2.752	2.714	2.856	2.798	2.814
$R_{Ct(N4)\ldots H(ax)}$, Å						0.594	
$R_{N\text{-}H(ax)}$, Å						2.114	
Ln-5d, e	0.89	1.27		0.92	1.26	0.99	0.80
Ln-4f, e	13.36	0.88		13.36	0.90	13.30	13.37
Q_{Ln}	2.06	2.01		2.08	2.01	2.06	2.04
E_{bind}(Ln-2P), eV	14.09	19.30		14.34[f]	19.00[f]	15.04[g]	18.80[h]
IP, eV	6.02 ($5a_2$)	6.17 ($5a_2$)				6.09 ($10a_2$)	
	6.11 ($11a_1$)	6.30 ($11a_1$)				6.30 ($23a_1$)	
	6.38 ($15e_2$/f)[i]					7.28 ($31e_1$/f)	
	6.54 ($16e_1$/f)						
	6.66 ($15e_3$/f)						
EA, eV	−2.98 ($5a_2$)	−2.12 ($15e_3$/f)				−2.54 ($15b_2$/f)	
	−2.28 ($12b_2$/f)	−1.23 ($16e_3$)					

[a] See legend of Table 1.

[b] X-ray crystal structure data on $Ce(OEP)_2$ (ref. 25)

[c] The second set of values represent the structural parameters related to the other, lower-part, porphyrin ring which does not carry an axial H atom (see Figure 1d).

[d] See legend of Table 1.

[e] $R_{P\text{-}P}$, which is equal to $2R_{Ct(N4)\ldots Ln}$, represents the distance between two porphines in the dimer.

[f] The value of binding energy for the positive ion is defined as $-E_{bind} = E([LnP_2]^+) - E(Ln^+) - 2E(P)$.

[g] Here $-E_{bind} = E(YbHP_2) - E(Yb) - 2E(P) - E(H)$.

[h] Here $-E_{bind} = E[(YbP_2)^-] - E(Yb^-) - 2E(P)$.

[i] Here "f" means an f-like orbital.

J Phys Chem A. Author manuscript; available in PMC 2008 December 8.

Table 4

Calculated excitation energies (E^{exc}) and oscillator strengths (*f*) for YbP(acac)

State	Contribution (%)[a]	E^{exc}, eV		*f*	Assignment[c]
		Calc	Exptl[b]		
1^2B_1	99 ($30a_1 \rightarrow 24b_1$)	0.15		0.2×10^{-4}	f → f
2^2B_1	90 ($29a_1 \rightarrow 24b_1$)	0.26		0.4×10^{-4}	f → f
3^2B_1	91 ($28a_1 \rightarrow 24b_1$)	0.42		0.3×10^{-4}	R → M
2^2A_1	79 ($22b_1 \rightarrow 24b_1$); 20 ($21b_1 \rightarrow 24b_1$)	0.75		0.0035	R → M
4^2A_1	71 ($21b_1 \rightarrow 24b_1$); 17 ($22b_1 \rightarrow 24b_1$)	1.71		0.0327	R → M
7^2B_1	96 ($25a_1 \rightarrow 24b_1$)	1.86		0.0041	R → M
9^2B_1	99 ($14a_2 \rightarrow 21b_2$)	2.06	2.08 (0.7)	0.4×10^{-7}	Q′
4^2B_2	99 ($14a_2 \rightarrow 25b_1$)	2.06		0.3×10^{-8}	
5^2A_1	93 ($19b_1 \rightarrow 24b_1$)	2.08		0.0049	R → M
8^2B_2	98 ($28a_1 \rightarrow 21b_2$)	2.58	2.23 (2.4)	0.0011	Q
13^2B_1	98 ($28a_1 \rightarrow 25b_1$)	2.58		0.0009	
10^2A_1	50 ($24b_1 \rightarrow 25b_1$); 39 ($20b_2 \rightarrow 21b_2$)	2.74		0.0014	M → R
15^2B_1	95 ($23a_1 \rightarrow 24b_1$)	2.83		0.0124	R → M
12^2B_2	99 ($23b_1 \rightarrow 15a_2$)	3.06		0.0015	
18^2B_1	66 ($19b_2 \rightarrow 15a_2$); 17 ($20b_2 \rightarrow 15a_2$)	3.13		0.0018	M → R
13^2B_2	43 ($28a_1 \rightarrow 21b_2$); 35 ($27a_1 \rightarrow 21b_2$)	3.15	2.90 (48)	0.1363	B
19^2B_1	52 ($28a_1 \rightarrow 25b_1$); 41 ($27a_1 \rightarrow 25b_1$)	3.17		0.0408	
19^2A_1	82 ($17b_2 \rightarrow 21b_2$)	3.21		0.0014	

State	Contribution (%)[a]	E^{exc}, eV		*f*	Assignment[c]
		Calc	Exptl[b]		
21^2B_1	67 ($27a_1 \rightarrow 25b_1$)	3.25	3.03 (5.0)	0.1202	B′
14^2B_2	60 ($27a_1 \rightarrow 21b_2$)	3.25		0.1635	
20^2A_1	87 ($13a_2 \rightarrow 15a_2$)	3.26		0.0049	M → R
23^2B_1	53 ($26a_1 \rightarrow 25b_1$)	3.29		0.2335	
16^2B_2	50 ($26a_1 \rightarrow 21b_2$); 11 ($27a_1 \rightarrow 21b_2$)	3.30		0.2058	
17^2B_2	74 ($11a_2 \rightarrow 24b_1$); 20 ($24b_1 \rightarrow 15a_2$)	3.33		0.0047	R → M
18^2B_2	62 ($24b_1 \rightarrow 15a_2$); 21 ($11a_2 \rightarrow 24b_1$)	3.35		0.0101	M → R
24^2B_1	49 ($26a_1 \rightarrow 25b_1$); 25 ($27a_1 \rightarrow 25b_1$)	3.36		0.1775	EB$_1$
19^2B_2	45 ($26a_1 \rightarrow 21b_2$); 17 ($27a_1 \rightarrow 21b_2$); 15 ($24b_1 \rightarrow 15a_2$)	3.37		0.1329	
25^2B_1	67 ($19b_2 \rightarrow 15a_2$); 19 ($20b_2 \rightarrow 15a_2$)	3.49		0.0019	
26^2B_1	55 ($18b_2 \rightarrow 15a_2$); 18 ($19b_2 \rightarrow 15a_2$)	3.57		0.0258	
21^2B_2	59 ($26a_1 \rightarrow 21b_2$); 22 ($23b_1 \rightarrow 16a_2$)	3.60		0.2301	EB_2

[a] Contribution of less than 10% is not listed; the same is true for other tables.

[b] Experimental data for YbTPP(acac), ref. [13]; the values in parentheses are the absorbance intensity ($\varepsilon 10^{-4}$) in $dm^3 mol^{-1} cm^{-1}$.

[c] M = metal and R = ring.

Table 5

Calculated excitation energies (E^{exc}) and oscillator strengths (*f*) for YbP_2

State	Contribution (%)	E^{exc}, eV		*f*	Assignment
		Calc	Exptl[a]		
1^3B_2	100 ($11a_1 \rightarrow 12b_2$)	0.11		0.0004	R → M
2^3B_2	93 ($5b_1 \rightarrow 5a_2$)	1.15	1.08 (3.83)	0.0713	near-IR
3^3E_1	98 ($14e_3 \rightarrow 12b_2$)	1.25		0.0016	R → M
3^3B_2	95 ($15e_3 \rightarrow 17e_1$) (β)	1.34		0.0117	M → R
6^3E_1	96 ($15e_1 \rightarrow 5a_2$)	1.50		0.0026	
4^3B_2	97 ($15e_3 \rightarrow 17e_1$) (α)	1.60		0.0043	M → R
5^3B_2	97 ($16e_1 \rightarrow 16e_3$)	1.63		0.0012	M → R
8^3E_1	75 ($12b_2 \rightarrow 16e_3$); 16 ($11b_2 \rightarrow 16e_3$)	1.73		0.0014	M → R
6^3B_2	99 ($10a_1 \rightarrow 12b_2$)	1.90		0.0171	R → M
11^3E_1	62 ($5a_2 \rightarrow 17e_1$); 29 ($14e_1 \rightarrow 5a_2$)	2.01	1.85 (3.21)	0.0030	Q_1
13^3E_1	56 ($14e_1 \rightarrow 5a_2$); 19 ($11a_2 \rightarrow 17e_1$); 16 ($5a_2 \rightarrow 17e_1$)	2.12		0.0040	
16^3E_1	68 ($5b_1 \rightarrow 16e_3$); 12 ($11a_1 \rightarrow 17e_1$)	2.34	2.34 (3.76)	0.0052	Q_2
18^3E_1	95 ($13e_3 \rightarrow 12b_2$)	2.51		0.0012	R → M
19^3E_1	95 ($11b_2 \rightarrow 16e_3$)	2.55	2.49 (3.75)	0.0018	Q_3
21^3E_1	92 ($12e_3 \rightarrow 12b_2$)	2.65		0.0098	R → M
23^3E_1	97 ($14e_2 \rightarrow 16e_3$)	2.81		0.0032	
11^3B_2	89 ($15e_1 \rightarrow 16e_3$)	3.08		0.0104	
26^3E_1	81 ($10b_2 \rightarrow 16e_3$)	3.13		0.0948	
28^3E_1	96 ($14e_2 \rightarrow 17e_1$)	3.29		0.0096	
13^3B_2	89 ($14e_3 \rightarrow 17e_1$)	3.41		0.0175	
29^3E_1	90 ($13e_2 \rightarrow 16e_3$)	3.61		0.0978	
30^3E_1	38 ($13e_2 \rightarrow 16e_3$); 33 ($16e_1 \rightarrow 16e_2$)	3.65	3.35 (4.98)	0.3866	B
31^3E_1	60 ($16e_1 \rightarrow 16e_2$); 31 ($13e_2 \rightarrow 16e_3$)	3.67		0.0662	
32^3E_1	33 ($13e_2 \rightarrow 16e_3$); 10 ($5b_1 \rightarrow 16e_3$)	3.74		0.7508	
16^3B_2	96 ($9a_1 \rightarrow 12b_2$)	3.75		0.0050	R → M
33^3E_1	95 ($10a_1 \rightarrow 17e_1$)	3.84		0.0192	

[a] Experimental data for $YbOEP_2$, ref. [22]; the values in parentheses are the absorbance intensity (log ε) in $dm^3mol^{-1}cm^{-1}$.

Table 6

Calculated excitation energies (E^{exc}) and oscillator strengths (*f*) for CeP_2

State	Contribution (%)	E^{exc}, eV		*f*	Assignment
		Calc	Exptl[a]		
1^1B_2	100 ($11a_1 \rightarrow 12b_2$)	0.87		0.0043	R → M
2^1B_2	93 ($15e_1 \rightarrow 15e_3$)	1.69		0.0038	R → M
3^1B_2	77 ($14e_2 \rightarrow 15e_2$); 20 ($14e_3 \rightarrow 16e_1$)	1.76		0.0011	R → M
7^1E_1	92 ($10b_2 \rightarrow 15e_3$)	1.78		0.0020	R → M
4^1B_2	79 ($14e_3 \rightarrow 16e_1$); 16 ($14e_2 \rightarrow 15e_2$)	1.87	1.94	0.0317	Q′
12^1E_1	68 ($5a_2 \rightarrow 17e_1$)	2.12	2.16	0.0102	Q
6^1B_2	99 ($13e_1 \rightarrow 15e_3$)	2.40		0.0069	R → M
7^1B_2	99 ($10a_1 \rightarrow 12b_2$)	2.56		0.0111	R → M
16^1E_1	93 ($13e_1 \rightarrow 15e_2$)	2.67	2.66	0.0096	Q″
18^1E_1	98 ($9b_2 \rightarrow 15e_3$)	2.81		0.0028	R → M
19^1E_1	95 ($14e_2 \rightarrow 16e_3$)	2.84		0.0090	
20^1E_1	84 ($13e_2 \rightarrow 16e_1$)	3.01		0.0526	R → M
8^1B_2	49 ($13e_2 \rightarrow 15e_2$); ($13e_2 \rightarrow 16e_1$)	3.05		0.0036	R → M
21^1E_1	97 ($13e_3 \rightarrow 15e_2$)	3.06		0.0024	R → M
9^1B_2	53 ($13e_3 \rightarrow 16e_1$); 24 ($15e_1 \rightarrow 16e_3$); 20 ($13e_2 \rightarrow 15e_2$)	3.07		0.0026	R → M
22^1E_1	55 ($10b_2 \rightarrow 16e_3$); 15 ($13e_3 \rightarrow 12b_2$); 11 ($13e_2 \rightarrow 16e_1$)	3.12		0.1190	
10^1B_2	50 ($15e_1 \rightarrow 16e_3$); 29 ($13e_2 \rightarrow 15e_2$); 13 ($14e_3 \rightarrow 17e_1$)	3.12		0.0223	
23^1E_1	79 ($13e_3 \rightarrow 12b_2$); 20 ($10b_2 \rightarrow 16e_3$)	3.17		0.0048	R → M
24^1E_1	94 ($14e_2 \rightarrow 17e_1$)	3.26		0.0224	
11^1B_2	82 ($14e_3 \rightarrow 17e_1$); 14 ($15e_1 \rightarrow 16e_3$)	3.38		0.0079	
25^1E_1	98 ($12e_2 \rightarrow 15e_3$)	3.39		0.0166	R → M
26^1E_1	33 ($12e_3 \rightarrow 15e_2$); 10 ($12e_3 \rightarrow 12b_2$); 10 ($10b_2 \rightarrow 16e_3$); 10 ($5b_1 \rightarrow 16e_3$)	3.54	3.28	0.9188	B
27^1E_1	54 ($12e_3 \rightarrow 15e_2$); 35 ($12e_3 \rightarrow 12b_2$)	3.64		0.1836	R → M
12^1B_2	91 ($13e_1 \rightarrow 16e_3$)	3.66		0.0101	
29^1E_1	48 ($12e_3 \rightarrow 12b_2$); 11 ($12e_3 \rightarrow 15e_2$)	3.80		0.8446	R → M
30^1E_1	92 ($10a_1 \rightarrow 17e_1$)	3.93		0.1212	

[a] Experimental data for $Ce(OEP)_2$, ref. [21].

Table 7

Calculated excitation energies (E^{exc}) and oscillator strengths (*f*) for $[CeP_2]^+$

State	Contribution (%)	E^{exc}, eV		*f*	Assignment
		Calc	Exptl[a]		
2^2B_2	89 ($11a_1 \rightarrow 12b_2$); 11 ($5b_1 \rightarrow 5a_2$)	0.81		0.0007	R → M
3^2B_2	85 ($5b_1 \rightarrow 5a_2$)	1.02	0.98	0.0573	near-IR
10^2E_1	53 ($15e_1 \rightarrow 5a_2$); 42 ($14e_1 \rightarrow 15e_3$)	1.43		0.0022	
5^2B_2	81 ($15e_1 \rightarrow 15e_3$); 15 ($14e_2 \rightarrow 15e_2$)	1.68		0.0028	R → M
14^2E_1	46 ($10b_2 \rightarrow 15e_3$); 26 ($14e_2 \rightarrow 16e_1$)	1.73		0.0032	R → M
9^2B_2	70 ($14e_3 \rightarrow 16e_1$); 10 ($14e_2 \rightarrow 15e_2$)	1.84		0.0453	R → M
21^2E_1	83 ($14e_1 \rightarrow 5a_2$)	1.95		0.0022	
25^2E_1	55 ($5a_2 \rightarrow 17e_1$); 14 ($5b_1 \rightarrow 16e_3$); 13 ($11a_2 \rightarrow 17e_1$); 11 ($13e_1 \rightarrow 5a_2$)	2.14		0.0042	
29^2E_1	39 ($5b_1 \rightarrow 16e_3$); 33 ($10a_1 \rightarrow 16e_1$)	2.38	2.41	0.0030	Q
30^2E_1	60 ($10a_1 \rightarrow 16e_1$); 31 ($5b_1 \rightarrow 16e_3$)	2.39		0.0044	R → M
13^2B_2	99 ($13e_1 \rightarrow 15e_3$)	2.43		0.0062	R → M
15^2B_2	97 ($10a_1 \rightarrow 12b_2$)	2.52		0.0137	R → M
34^2E_1	56 ($13e_1 \rightarrow 15e_2$); 31 ($14e_2 \rightarrow 16e_3$)	2.69		0.0040	R → M
35^2E_1	57 ($14e_2 \rightarrow 16e_3$); 39 ($13e_1 \rightarrow 15e_2$)	2.70		0.0068	R → M
38^2E_1	94 ($14e_2 \rightarrow 16e_3$)	2.80		0.0072	
40^2E_1	98 ($9b_2 \rightarrow 15e_3$)	2.84		0.0048	R → M
41^2E_1	96 ($10b_2 \rightarrow 16e_3$)	2.98		0.0036	
42^2E_1	51 ($13e_2 \rightarrow 16e_3$); 26 ($10b_2 \rightarrow 16e_3$)	3.01		0.0682	
43^2E_1	97 ($13e_2 \rightarrow 16e_1$)	3.02		0.0032	R → M
45^2E_1	47 ($10b_2 \rightarrow 16e_3$); 45 ($13e_2 \rightarrow 16e_1$)	3.08		0.0116	
48^2E_1	96 ($13e_2 \rightarrow 12b_2$) (β)	3.16		0.0162	R → M
49^2E_1	95 ($13e_3 \rightarrow 12b_2$) (α)	3.23		0.0282	R → M
50^2E_1	94 ($14e_2 \rightarrow 17e_1$)	3.25		0.0308	
52^2E_1	99 ($12e_2 \rightarrow 15e_3$)	3.44		0.0132	R → M
53^2E_1	31 ($12e_3 \rightarrow 15e_2$); 12 ($5b_1 \rightarrow 16e_3$); 10 ($12e_3 \rightarrow 12b_2$)	3.57	3.44	0.9930	B
54^2E_1	98 ($12e_3 \rightarrow 15e_2$)	3.59		0.0166	R → M
56^2E_1	51 ($12e_3 \rightarrow 15e_2$); 33 ($12e_3 \rightarrow 12b_2$)	3.67		0.1830	R → M
60^2E_1	49 ($12e_3 \rightarrow 12b_2$)	3.84		0.7058	R → M

[a] Experimental data for $[Ce(OEP)_2]^+$, ref. [20] and ref. [21].

Table 8

Calculated excitation energies (E^{exc}) and oscillator strengths (*f*) for $YbHP_2$

State	Contribution (%)	E^{exc}, eV		*f*	Assignment
		Calc	Exptl[a]		
3^2E	88 ($29e \rightarrow 15b_2$)	0.49		0.0036	R → M
1^2A_1	91 ($14b_2 \rightarrow 15b_2$)	0.77		0.0030	R → M
5^2E	100 ($27e \rightarrow 15b_2$)	1.23		0.0014	R → M
3^2A_1	97 ($23a_1 \rightarrow 24a_1$)	1.51		0.0253	$R \rightarrow H_{(ax)}$
5^2A_1	70 ($13b_2 \rightarrow 15b_2$); 19 ($22a_1 \rightarrow 24a_1$)	1.84		0.0140	R → M
15^2E	69 ($10a_2 \rightarrow 33e$)	2.12	2.04 (3.50)	0.0068	Q_1
19^2E	73 ($22a_1 \rightarrow 32e$)	2.25	2.23 (3.87)	0.0003	Q_2
27^2E	69 ($22a_1 \rightarrow 33e$)	2.59	2.53 (3.92)	0.0034	Q_3
28^2E	47 ($21a_1 \rightarrow 32e$); 22 ($15b_2 \rightarrow 32e$)	2.64		0.0086	M → R
33^2E	24 ($28e \rightarrow 24a_1$); 23 ($21a_1 \rightarrow 32e$); 15 ($29e \rightarrow 24a_1$)	2.78		0.0296	$R \rightarrow H_{(ax)}$
15^2A_1	82 ($29e \rightarrow 32e$); 10 ($31e \rightarrow 32e$)	2.83		0.0050	
37^2E	93 ($28e \rightarrow 24a_1$)	2.98		0.0030	$R \rightarrow H_{(ax)}$
38^2E	35 ($14b_1 \rightarrow 32e$); 33 ($15b_1 \rightarrow 32e$)	3.00		0.0054	
41^2E	44 ($21a_1 \rightarrow 33e$); 25 ($20a_1 \rightarrow 32e$); 12 ($9a_2 \rightarrow 33e$)	3.06		0.0058	M → R
42^2E	82 ($14b_1 \rightarrow 32e$)	3.08		0.0060	
44^2E	40 ($21a_1 \rightarrow 33e$); 25 ($9a_2 \rightarrow 33e$)	3.17	3.06 (5.42)	0.0376	B
45^2E	54 ($14b_2 \rightarrow 33e$); 39 ($15b_2 \rightarrow 33e$)	3.21		0.0016	
47^2E	75 ($27e \rightarrow 24a_1$); 19 ($21a_1 \rightarrow 33e$)	3.28		0.0128	$R \rightarrow H_{(ax)}$
49^2E	51 ($21a_1 \rightarrow 33e$); 11 ($20a_1 \rightarrow 33e$)	3.34		0.0050	
51^2E	68 ($14b_1 \rightarrow 33e$); 23 ($15b_1 \rightarrow 33e$)	3.40		0.0026	
54^2E	96 ($23e \rightarrow 15b_2$)	3.54		0.0012	R → M
55^2E	41 ($20a_1 \rightarrow 33e$)	3.60		0.2274	EB_1
56^2E	91 ($19a_1 \rightarrow 32e$)	3.63		0.0130	
57^2E	100 ($22e \rightarrow 15b_2$)	3.71		0.0018	R → M
58^2E	40 ($20a_1 \rightarrow 33e$)	3.73		0.6314	EB_2

[a] Experimental data for $YbH(TPP)_2$, ref. [29]; the values in parentheses are the absorbance intensity (log ε) in $dm^3mol^{-1}cm^{-1}$.

Table 9

Calculated excitation energies (E^{exc}) and oscillator strengths (*f*) for $[YbP_2]^-$

State	Contribution (%)	E^{exc}, eV		*f*	Assignment
		Calc	Exptl[a]		
1^2B_2	100 ($11a_1 \rightarrow 12b_2$)	0.17		0.0024	R → M
2^2B_2	100 ($15e_3 \rightarrow 17e_1$)	1.21		0.0026	M → R
3^2E_1	98 ($14e_3 \rightarrow 12b_2$)	1.28		0.0016	
3^2B_2	99 ($15e_3 \rightarrow 17e_1$)	1.54		0.0016	M → R
5^2B_2	100 ($10a_1 \rightarrow 12b_2$)	1.93		0.0092	R → M
11^2E_1	71 ($5a_2 \rightarrow 17e_1$); 12 ($11a_1 \rightarrow 17e_1$)	2.07	1.94 (3.46)	0.0082	Q_1
13^2E_1	70 ($5b_1 \rightarrow 16e_3$); 18 ($11a_1 \rightarrow 17e_1$)	2.24	2.03 (3.48)	0.0007	Q_2
14^2E_1	66 ($5b_1 \rightarrow 16e_3$); 24 ($11a_1 \rightarrow 17e_1$)	2.28	2.21 (3.90)	0.0042	Q_3
17^2E_1	96 ($11b_2 \rightarrow 16e_3$)	2.54	2.37 (3.80)	0.0020	Q_4
18^2E_1	91 ($12e_3 \rightarrow 12b_2$)	2.63	2.53 (4.12)	0.0158	Q_5
20^2E_1	96 ($14e_2 \rightarrow 16e_3$)	2.77	2.62 (4.15)	0.0028	Q_6
10^2B_2	88 ($15e_1 \rightarrow 16e_3$); 11 ($14e_3 \rightarrow 17e_1$)	3.03		0.0070	
23^2E_1	82 ($10b_2 \rightarrow 16e_3$); 17 ($14e_2 \rightarrow 17e_1$)	3.11		0.0014	
24^2E_1	75 ($10b_2 \rightarrow 16e_3$)	3.14	3.05 (5.67)	0.1516	B
25^2E_1	94 ($14e_2 \rightarrow 17e_1$)	3.19		0.0026	
12^2B_2	87 ($14e_3 \rightarrow 17e_1$); 10 ($15e_1 \rightarrow 16e_3$)	3.34		0.0128	
26^2E_1	80 ($13e_2 \rightarrow 16e_3$); 16 ($16e_1 \rightarrow 16e_2$)	3.54		0.0248	
27^2E_1	74 ($16e_1 \rightarrow 16e_2$); 21 ($13e_2 \rightarrow 16e_3$)	3.55		0.0600	M → R
28^2E_1	70 ($13e_2 \rightarrow 16e_3$)	3.58		0.3006	EB_1
29^2E_1	26 ($13e_2 \rightarrow 16e_3$); 12 ($5b_1 \rightarrow 16e_3$); 10 ($10b_2 \rightarrow 16e_3$)	3.67		0.9008	EB_2

[a] Experimental data for $[Yb(TPP)_2]^-$, ref. [29]; the values in parentheses are the absorbance intensity (log ε) in $dm^3mol^{-1}cm^{-1}$.